



OPEN ACCESS

EDITED BY

Xiaojian Zhu,
Chinese Academy of Sciences (CAS),
China

REVIEWED BY

Xiaobing Yan,
Hebei University, China
Dashan Shang,
Institute of Microelectronics (CAS),
China

*CORRESPONDENCE

Ye Tao
taoy506@nenu.edu.cn
Zhongqiang Wang
wangzq752@nenu.edu.cn

RECEIVED 10 August 2022

ACCEPTED 29 August 2022

PUBLISHED 14 September 2022

CITATION

Xin X, Sun L, Chen J, Bao Y, Tao Y,
Lin Y, Bian J, Wang Z, Zhao X, Xu H and
Liu Y (2022) Real-time numerical
system convertor *via* two-dimensional
WS₂-based memristive device.
Front. Comput. Neurosci. 16:1015945.
doi: 10.3389/fncom.2022.1015945

COPYRIGHT

© 2022 Xin, Sun, Chen, Bao, Tao, Lin,
Bian, Wang, Zhao, Xu and Liu. This is
an open-access article distributed
under the terms of the [Creative
Commons Attribution License \(CC BY\)](#).
The use, distribution or reproduction in
other forums is permitted, provided
the original author(s) and the copyright
owner(s) are credited and that the
original publication in this journal is
cited, in accordance with accepted
academic practice. No use, distribution
or reproduction is permitted which
does not comply with these terms.

Real-time numerical system convertor *via* two-dimensional WS₂-based memristive device

Xing Xin, Liyao Sun, Jiamei Chen, Youzhe Bao, Ye Tao*,
Ya Lin, Jingyao Bian, Zhongqiang Wang*, Xiaoning Zhao,
Haiyang Xu and Yichun Liu

Center for Advanced Optoelectronic Functional Materials Research, Key Laboratory of UV-Emitting Materials and Technology, Ministry of Education, Northeast Normal University, Changchun, China

The intriguing properties of two-dimensional (2D) transition metal dichalcogenides (TMDCs) enable the exploration of new electronic device architectures, particularly the emerging memristive devices for in-memory computing applications. Implementation of arithmetic logic operations taking advantage of the non-linear characteristics of memristor can significantly improve the energy efficiency and simplify the complexity of peripheral circuits. Herein, we demonstrate an arithmetic logic unit function using a lateral volatile memristor based on layered 2D tungsten disulfide (WS₂) materials and some combinational logic circuits. Removable oxygen ions were introduced into WS₂ materials through oxygen plasma treatment process. The resistive switching of the memristive device caused by the thermophoresis-assisted oxygen ions migration has also been revealed. Based on the characteristics of excitatory postsynaptic current (EPSC), paired-pulse facilitation (PPF), and spike rate dependent plasticity (SRDP), a real-time numerical system convertor was successfully accomplished, which is a significant computing function of arithmetic logic unit. This work paves a new way for developing 2D memristive devices for future arithmetic logic applications.

KEYWORDS

memristor, numerical system convertor, oxygen plasma, transition metal dichalcogenides, tungsten disulfide

Introduction

The explosive increase of data along with the rapid development of big data analytics and internet of things demands innovative device architectures and alternative materials (Li et al., 2018; Dai et al., 2019; Zhu et al., 2019). In-memory computing, which can process and store information simultaneously, has the potential to address the critical challenge affecting current computing platforms (von Neumann computer architecture) (Ielmini and Wong, 2018; Jain et al., 2018; Aqib et al., 2019; Verma et al., 2019).

Memristor, possessing the characteristics of simple structure, low power consumption and non-linear conductance variation, can be employed to accomplish some interesting computing functions, such as arithmetical computing, logical operation, and reservoir computing application (Hu et al., 2018; Mao et al., 2019; Choi et al., 2020; Lin et al., 2020; Zhong et al., 2021). Introducing these memristive devices will not only greatly simplify the peripheral circuit complexity, but also effectively improve the energy consumption and back-end integration potential (Kumar et al., 2022). A more advanced computing function of arithmetic logic unit (ALU) has also been proposed to further improve the development of in-memory computing (Cheng et al., 2019).

Two-dimensional (2D) materials, such as transition metal dichalcogenides (TMDCs), have attracted numerous attention and accelerated the progress of memristive devices in both the storage and computing applications in recent years (Chia and Pumera, 2018; Akinwande et al., 2019; Li et al., 2019; Liu et al., 2019, 2020; Yang et al., 2019; Chen et al., 2020; Wang et al., 2020; Zavabeti et al., 2020; Zhou et al., 2021; Kwon et al., 2022). Wang et al. (2018) have reported a robust layered $\text{MoS}_{2-x}\text{O}_x$ -based memristor through the oxidation of MoS_2 films in ambient air. The obtained device exhibited an excellent switching performance with an endurance of $\sim 10^7$ and an ultra-high operating temperature of 340°C (Wang et al., 2018). Lin et al. have used a self-oxidized method to fabricate a stable unipolar switching $\text{MoS}_2/\text{graphene}/\text{HfSe}_{2-x}\text{O}_x$ memristor (Yin et al., 2020). It possessed the ability for the multi-bit data storage and could also be acted as a memory latch or logic gate. In addition, versatile memristive behaviors and functions with dual-mode operation (electrical and optical stimuli) could also be realized, according to the outstanding photoelectrical characteristics of 2D materials. A dynamic memristive device based on 2D tin sulfide (SnS_2) materials has been built by Sun et al. (2021) demonstrating the optoelectronic reservoir computing for language learning function. It is obvious to see that adjusting the micro-structure of 2D materials is an efficient way to control the properties of memristive devices based on them, which would thereby further widen their application range.

In addition, the implementation of arithmetic logic functions within the memristors is one of the most significant extended applications for in-memory computing. Cheng et al. (2019) have demonstrated several arithmetic logic unit functions through a memristive crossbar, including non-volatile Boolean logic and arithmetic computing, which improves the development of in-memristor computing. In fact, the numerical system convertor as another kind of arithmetic logic operations, which contains binary-to-decimal, binary-to-hexadecimal and decimal-to-hexadecimal types et al., was also usually executed in the arithmetic logic unit (ALU) (Sharma and Kumre, 2020). However, the investigations about the achievement

of numerical system convertors through a memristor-based computing architectures have been rarely reported.

WS_2 , a typical semiconductor material with tunable band gap (1.2~2.1 eV) from multilayer to monolayer (Kuc et al., 2011), possesses high phonon limited electron mobility (Zhang et al., 2014), on/off current ratio (Yue et al., 2018) and light effective mass (Liu et al., 2011), which enable it to apply to low-power memristors as active layer (Luo et al., 2020). Especially, the existence of sulfur vacancies in WS_2 will introduce localized donor states inside the bandgap, which largely changes its carrier mobility and memristive behavior. Herein, we will demonstrate a lateral memristor based on oxygen-plasma-treated 2D tungsten disulfide (WS_2) materials. It is worth emphasizing that the corresponding memristive behaviors can be continuously regulated by changing the duration time of oxygen plasma treatment. Because of a lower migration barrier for oxygen ions than that for sulfur ions (Wang et al., 2018), the doped oxygen ions could thermophoresis-assisted migrate under an electric field. Some synapse-based electrical characteristics, excitatory postsynaptic current (EPSC), paired-pulse facilitation (PPF), and spike rate dependent plasticity (SRDP) have been efficiently emulated. In addition, a real-time numerical system convertor was also successfully accomplished, according to the unique accumulation and relaxation characteristics of the 2D WS_2 materials-based memristor. It has not been demonstrated with 2D TMDCs memristor before and these results will provide a potential approach for the development of future arithmetic logic unit.

Materials and methods

Device fabrication

Firstly, the Au electrode with interdigital structure was fabricated through the technology of standard lithography and thermal evaporation. Subsequently, the layered 2D WS_2 was mechanically exfoliated with the assistance of accurate two-dimensional transfer platform (METATEST E1-T). The schematic diagram of device structure is shown in **Figure 1A**. In order to introduce the sulfur vacancies and oxygen elements into the layered WS_2 without completely damaging the material micro-structure, a soft oxygen plasma treatment was conducted under a power of 30 W with variable treatment durations (<90 s).

Characterization and electrical measurements

The AFM measurements were performed in air using a Bruker Dimension Icon atomic force microscope (Bruker, Germany). The X-ray photoelectron spectroscopy (XPS) was

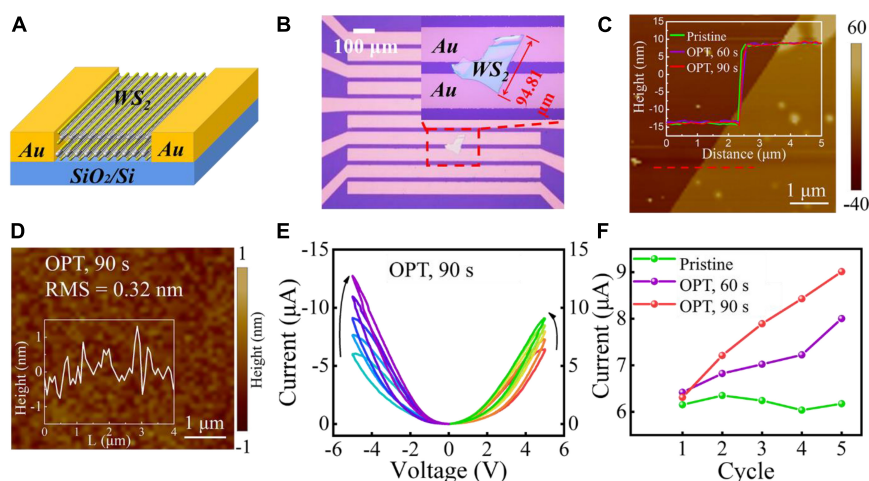


FIGURE 1

(A) A schematic diagram of the lateral Au/WS₂/Au device. (B) A microscopic image of the lateral memristive device with interdigital electrodes. (C) The AFM height topography measured at the edge of WS₂ flake. The inset shows the height profiles measured along the red dotted line in panel (D), illustrating the thickness variation of pristine WS₂ and oxygen-plasma-treated WS₂. (D) AFM morphology of the layered WS₂ experiencing OPT for 90 s. The root-mean-square (RMS) roughness value is also presented. The inset is the representative height line scan. (E) Typical I-V curves of the memristive device after OPT for 90 s. (F) Variation trend of the maximal current value with continuous 5 cycles of pristine devices and after OPT for 60 and 90 s, respectively.

performed on an ESCA-LAB 250 photoelectron spectrometer equipped with X-ray source in Al $k\alpha$ (1486.7 eV). The atomic structure of high-quality single-crystal WS₂ domain was carried out by TEM on an FEI Titan Themis Cube with an X-FEG electron gun operating at 100 kV. Raman spectra was recorded with a JY HR-800 LabRam Infinity Spectrophotometer with a 488 nm semiconductor laser. The X-ray diffraction (XRD) measurements were conducted using Dmax-2500X (Rigaku, Japan). All the electrical measurements were performed with a source meter (2636A, Keithley), an arbitrary function generator (3390, Keithley), and an oscilloscope (TDS 2012B, Tektronix), and the testing environment was maintained under temperature of $\sim 25^\circ\text{C}$ and relative humidity of $\sim 30\%$.

Results and discussion

The schematic diagram of device structure and the interdigital electrode structure fabricated through standard lift-off lithography technology are shown in **Figures 1A,B**. This structure makes the WS₂ multilayers and electrodes to form a lateral Au/WS₂/Au memristive device with a channel width of $\sim 20\ \mu\text{m}$. For adjusting the micro-structure of the mechanically exfoliated multilayer WS₂ flakes, the lateral memristive device was treated by a soft oxygen plasma. It was implemented by a source located far from the sample with a low power (30 W) and short exposure time ($< 90\ \text{s}$). The variation of the micro-structure, physical and chemical properties of WS₂ induced by the different oxygen plasma exposure times was investigated thoroughly. As shown in **Figure 1C**, the thicknesses

($\sim 22.5\ \text{nm}$) of multilayer WS₂ changed a little after the oxygen plasma treatment (OPT), which were measured at the flake edge by atomic force microscope (AFM). **Figure 1D** and **Supplementary Figure 1** show the surface morphology of pristine WS₂ and WS₂ flakes treated by oxygen plasma for 60 and 90 s. The corresponding root-mean-square (RMS) roughness values are 0.15, 0.23, and 0.32 nm, respectively. The roughness of WS₂ flake treated by oxygen plasma for 90 s increased slightly (0.17 nm), compared with that of pristine WS₂. This phenomenon is consistent with the unobvious variation of the WS₂ thickness after oxygen plasma treatment in **Figure 1C**. The representative line scans extracted from the AFM maps (Insets in **Figure 1D** and **Supplementary Figure 1**) show that the peak-to-valley height excursion (HE) increases with prolonging oxygen plasma exposure time. The HE value is less than the thickness of monolayer WS₂ ($\sim 0.7\ \text{nm}$) for 60 s treatment. When exposure time was up to 90 s, the HE value increased to $\sim 1\ \text{nm}$. It means that maybe a small amount of structural damage was introduced by a long-time OPT. As reported, when performing energetic plasma treatments, the exposed multilayer TMDCs may undergo a significant etching (Chen et al., 2013; Giannazzo et al., 2017). To forbid a more serious damage of WS₂, oxygen plasma exposure time was controlled within 90 s in our experiments. **Figure 1E** shows the typical I-V curves of the lateral Au/WS₂/Au memristive device after OPT for 90 s, from which we can see that the treated memristor shows an analogy memristive behavior. The current amplitudes would both increase along with either positive or negative DC voltage sweeping operations, which could result from the same Au noble electrodes. In contrast, as shown in

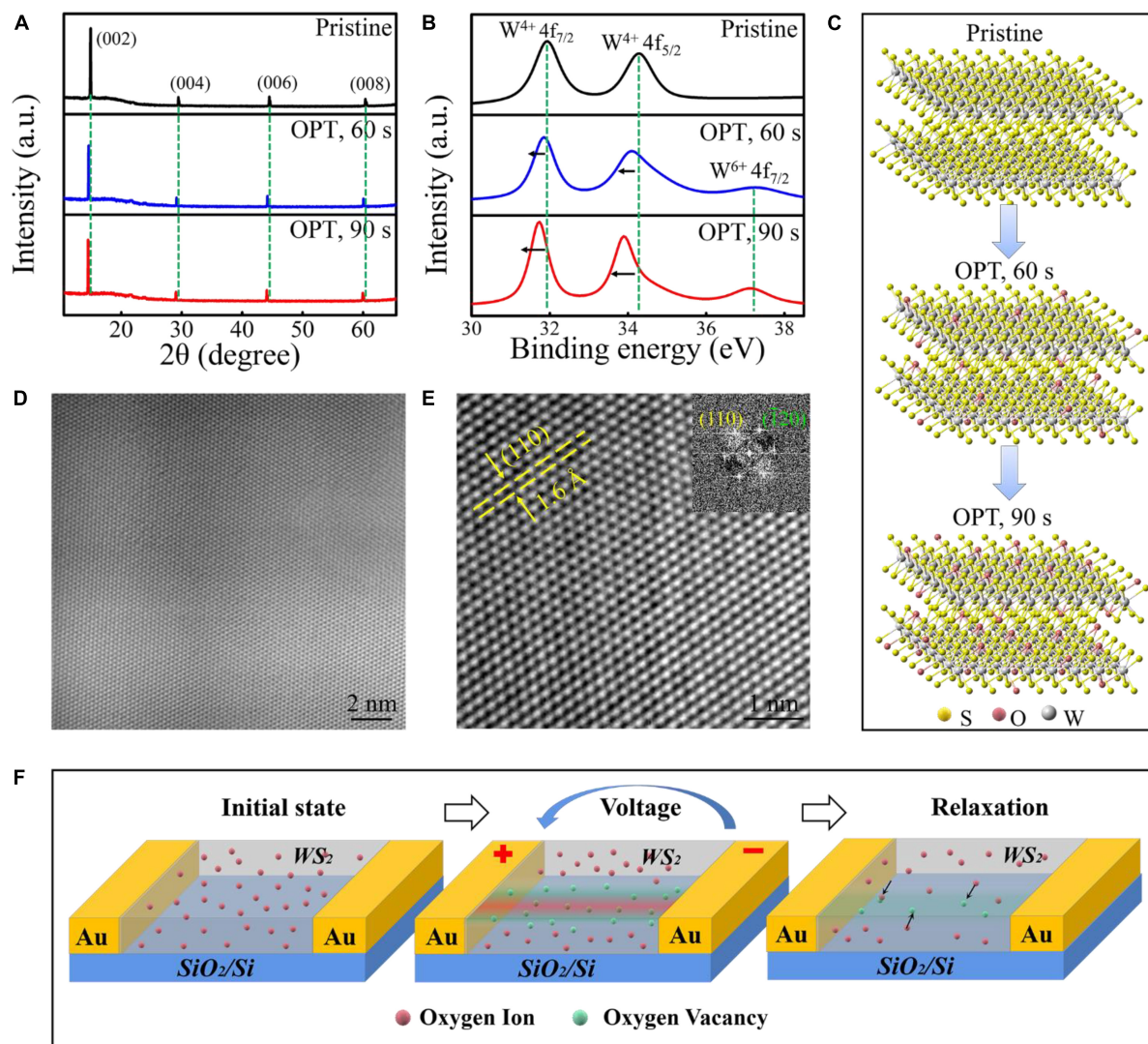


FIGURE 2 (A) XRD and (B) XPS spectra of WS_2 before and after oxygen plasma treatment for 60 and 90 s. (C) The structural schematic diagram for the variation of multilayer WS_2 with different oxygen plasma exposure times. HRTEM images at (D) low and (E) high magnification performed at multilayer WS_2 interior after oxygen plasma treatment for 90 s. The inset in panel (E) is the corresponding FFT image. (F) A schematic diagram for the memristive mechanism of the lateral memristive device.

Figure 1F and Supplementary Figure 2, there exists no obvious memristive behavior although continuous DC voltage sweep was operated on both the pristine and 60 s-OPT devices. The related physical mechanism will be discussed as follows.

For investigating thoroughly, the effect on the memristive characteristic of the lateral Au/ WS_2 /Au device from oxygen plasma treatment, the X-ray diffraction (XRD) measurements were conducted as shown in Figure 2A. There are four main peaks for pristine multilayer WS_2 , which locate at 14.4° (002), 28.9° (004), 44.0° (006), and 59.9° (008), respectively. After OPT for 60 and 90 s, every WS_2 peak has a left shift compared to pristine WS_2 peaks. These results illustrate that the WS_2 crystal structure was unchanged after OPT. Instead, it proves

that oxygen plasma will introduce oxygen doping into WS_2 , which induced the increase of lattice spacing and the left shift of WS_2 peaks. The Raman spectra in Supplementary Figure 3 also present the same conclusion. Then, we conducted the X-ray photoelectron spectroscopy (XPS) measurements to further confirm the successful oxygen doping of WS_2 by oxygen plasma (Figure 2B). It has been reported that some oxygen ions may also be injected to dope the sulfur vacancies (Esfandiari and Mohajerzadeh, 2019; Esfandiari et al., 2020). It is worth noting that the peak at 37.2 eV after OPT corresponds to the binding energy of W^{6+} , indicating the oxidation and doping of WS_2 . The binding energy of W^{4+} of pristine WS_2 decrease after oxygen plasma, suggesting the electron transfer from W^{4+} to W^{6+} .

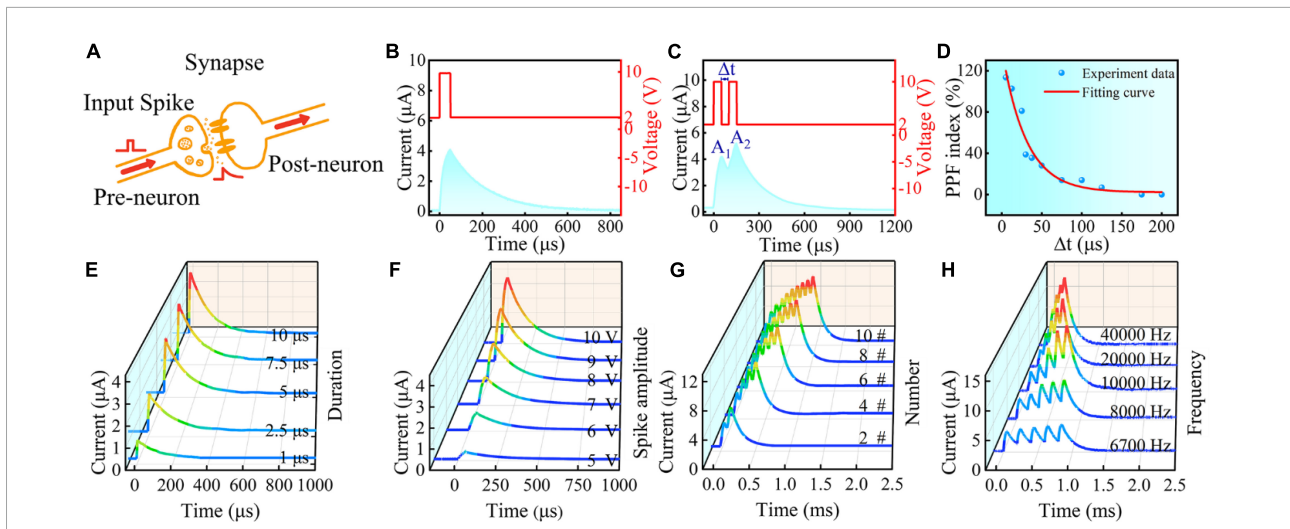


FIGURE 3 (A) Illustrations of the biological synapse based on the WS₂ memristor after OPT for 90 s. Current response of the lateral Au/WS₂/Au memristor under (B) a single spike and (C) paired spikes. (D) PPF index versus the relative spike timing. Current response under a single spike with (E) different duration times and (F) amplitude of input spikes. Current response under (G) different spike numbers and (H) different frequencies.

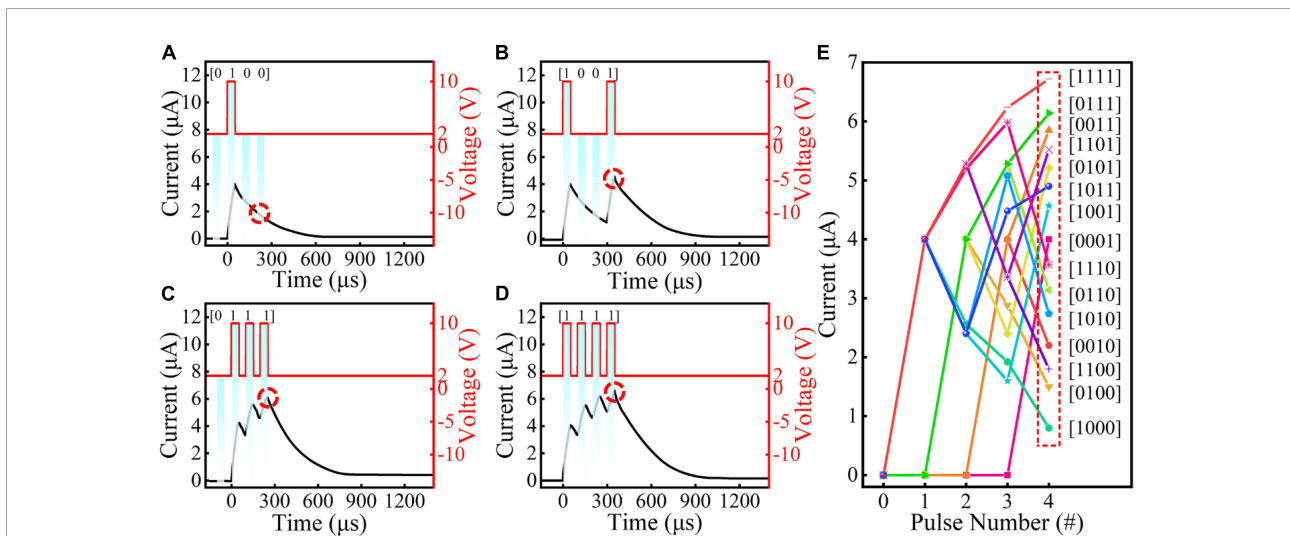
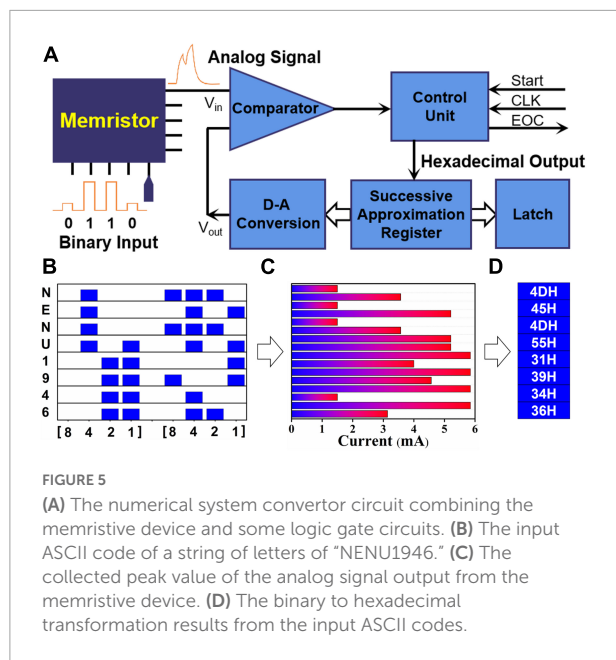


FIGURE 4 (A–D) The current response of the lateral Au/WS₂/Au memristive device to 4 different pulse streams: [0100], [1001], [0111] and [1111], respectively. (E) 16 peak current distribution of the memristive device with 16 kinds of 4 bits binary coding.

We have used a schematic diagram to intuitively exhibit the structure evolution with different oxygen plasma exposure times (Figure 2C). Figures 2D,E are the high-resolution transmission electron microscopy (HRTEM) images detected at WS₂ flake after oxygen plasma treatment for 90 s. The distance of the (110) plane with the value of 1.6 Å was identified by a fast Fourier transform (FFT) image as shown in the inset of Figure 2E, which was in good agreement with its theoretical value. The contrast in HRTEM image is related to the stacking of columns of S and W atoms in multilayer WS₂. Due to the low atomic numbers of oxygen, O atoms in WS₂ are invisible. However,

the results show the WS₂ lattice was slightly affected by the soft OPT. Figure 2F shows the memristive mechanism for the lateral memristive device. The oxygen ions distribute uniformly in the surface of 2D WS₂ materials after the oxygen plasma treatment. Comparing with the inherent sulfur ions, the doped oxygen ions possess a lower migration barrier (Wang et al., 2018). Therefore, under an electric field, the oxygen ions could gradually migrate toward the anode since thermophoresis effect would dominate due to the steep radial temperature gradient produced by Joule heating (Wang et al., 2018). The resistive switching mechanism primarily based on the high conductive oxygen vacancies region



evolution. In addition, the short time relaxation process after removing the voltage pulse maybe caused by the recombination of oxygen ions around oxygen vacancies region.

Such gradual change behavior of conductance in the lateral Au/WS₂/Au memristive device is just appropriate for emulating the synaptic learning functions. As shown in **Figure 3A**, the synaptic weight could be continuously adjusted through various input spikes. The current response of this memristor under a single spike (10 V, 50 μs) was shown in **Figure 3B**. We can see that the square pulse triggered an abrupt increase of current signal, and then subsequently recovered to the initial state. Such characteristic is very similar to the excitatory postsynaptic current (EPSC) phenomenon of biological synapse. Interestingly, the relaxation process of current signal provides the basis for achieving temporal correlation between two neighboring spikes. One typical temporal correlation between spikes is the paired-pulse facilitation (PPF) function, which is demonstrated in **Figure 3C**. Apparently, the EPSC value after the second spike is larger than that of the first one, which exactly reflects the PPF effect of the biological synapse. The PPF effect becomes weaker with increasing interval time, as presented by the PPF index in **Figure 3D**. The current response of the memristor under different single spike and multiple spikes was also investigated. **Figures 3E,F** show the current variation with different duration times and amplitude of input spikes, from which we can see that a longer or larger input spike will trigger a higher current signal. However, the relaxation time after different stimulus intensity did not show a significant variation. Correspondingly, the peak value of the EPSC shows an obvious increase with more spike numbers and higher frequencies (**Figures 3G,H**), which can be used to realize the

high-pass frequency filter. These essential electrical properties provide the basis for the following numerical system convertor application.

Taking advantage of the current response of the lateral Au/WS₂/Au memristive device to different stimulus intensity, especially to the spiking number and frequency, we have conducted the response experiments of a series of 4 bits binary coding. As shown in **Figures 4A–D**, extensive tests were carried out to characterize the memristor response to different temporal inputs. We can see that the current response processes to different binary coding ([0100], [1001], [0111], and [1111]) are unique. Thus, it is expected that the read current (immediately after the pulse train), can also be well distinguished between the different binary coding. We have further collected 16 current response results for all 4 bits binary coding to verify this speculation (**Figure 4E**). This interesting gradual accumulation and relaxation behaviors can also be used for the reservoir computing application.

The up-to-date computers are all based on binary computing and storage systems. Numerical system convertor is a significant computational function of arithmetic logic unit (ALU) of central processing unit (CPU). Especially, the transformation between binary and hexadecimal is one of the most commonly used numerical convertor process, such as the compilation process of assembler source program. That is, the numerical system convertor process needs to occupy the system bus of computer system. Therefore, it is extremely willing to implement the numerical system convertor *via* several electron devices or logic gate circuits only. Herein, according to the current response characteristics of our lateral Au/WS₂/Au memristive device, the numerical convertor operation from binary to hexadecimal has been realized. As shown in **Figure 5A**, we have designed the numerical convertor circuit with some basic function modules. A 4-bit binary signal, which can be regarded as the input signal (V_{in}) of the numerical convertor circuit, was firstly imported into the memristive device. Then, an analog signal outputs from the other electrode. The numerical converting operation was activated by the start signal. The highest order of the successive approximation register is set to "1" (high level), and all the others are set to "0" (low level). At this point, the output voltage (V_{out}) is half of the full range. Through the comparison process, the highest order was maintained as "1" if the V_{out} signal was smaller than the V_{in} signal, which is the maximum value of the output signal of the memristive device, and vice versa. Once the V_{in} signal is smaller than that of the full range, the second high order will be set to "1." It will be judged if the V_{in} signal is larger than quarter of the full range. The hexadecimal number can be confirmed by only 4 times recurrence. After a series of comparison operation, the control circuit will output the signal of End of Conversion (EOC). Subsequently, the final contents in the successive approximation register will be transmitted into the latch as the result of numerical converting operation.

As shown in **Figure 5B**, a string of letters of “NENU1946” were programmed into our lateral Au/WS₂/Au memristive device in the form of American standard code for information interchange (ASCII) code. Through extracting the peak value of the output analog signal, the maximal current value was collected as shown in **Figure 5C**. The hexadecimal number of the letters of “NENU1946,” which is 4DH, 45H, 4DH, 55H, 31H, 39H, 34H, and 35H, are successfully converted in **Figure 5D**. The above results demonstrate that the numerical system convertor could be realized through the 2D memristive device integrated with several logic gate circuits.

Conclusion

In summary, a binary-to-hexadecimal numerical system convertor was successfully achieved based on the especial current response characteristics of the lateral Au/WS₂/Au memristive device. The 2D WS₂ based memristive device was fabricated through standard lift-off lithography and mechanically exfoliation technologies. The memristive characteristics of our lateral device could be continuously regulated with oxygen plasma treatment time. Several essential synaptic functions, such as EPSC, PPF and SRDP were demonstrated in the memristive device. In addition, this 2D WS₂ based device could be used in numerical system convertor application only integrating with some combinational logic circuits. This work provides a feasible idea for enabling 2D memristor to accomplish the arithmetic application, which will further broaden the scope for in-memory computing.

Data availability statement

The original contributions presented in this study are included in the article/**Supplementary material**, further inquiries can be directed to the corresponding authors.

Author contributions

All authors listed have made a substantial, direct, and intellectual contribution to the work, and approved it for publication.

References

Akinwande, D., Huyghebaert, C., Wang, C. H., Serna, M. I., Goossens, S., Li, L. J., et al. (2019). Graphene and two-dimensional materials for silicon technology. *Nature* 573, 507–518. doi: 10.1038/s41586-019-1573-9

Funding

This work was supported by the fund from the Ministry of Science and Technology of China (Nos. 2019YFB2205100 and 2021YFA0716400), the NSFC for Distinguished Young Scholars (No. 52025022), the Program of National Natural Science Foundation of China (Nos. 11974072, 52072065, 51732003, 51872043, 51902048, 62004016, 52002056, and U19A2091), the “111” Project (No. B13013), the funding from Jilin Province (Nos. 20210509045RQ, YDZJ202101ZYTS021, 2412021ZD003, YDZJ202101ZYTS046, and 20210201062GX), and the Fundamental Research Funds for the Central Universities (Nos. 2412022QD036 and 2412021ZD006).

Acknowledgments

We sincerely acknowledged H. Zhu and G. Wang for providing technology supporting on characterization of the samples.

Conflict of interest

The authors declare that the research was conducted in the absence of any commercial or financial relationships that could be construed as a potential conflict of interest.

Publisher's note

All claims expressed in this article are solely those of the authors and do not necessarily represent those of their affiliated organizations, or those of the publisher, the editors and the reviewers. Any product that may be evaluated in this article, or claim that may be made by its manufacturer, is not guaranteed or endorsed by the publisher.

Supplementary material

The Supplementary Material for this article can be found online at: <https://www.frontiersin.org/articles/10.3389/fncom.2022.1015945/full#supplementary-material>

Aqib, M., Mehmood, R., Alzahrani, A., Katib, I., Albeshri, A., and Altowajiri, S. M. (2019). Smarter traffic prediction using big data, in-memory computing, deep learning and GPUs. *Sensors* 19:2206. doi: 10.3390/s19092206

- Chen, M., Nam, H., Wi, S., Ji, L., Ren, X., Bian, L., et al. (2013). Stable few-layer MoS₂ rectifying diodes formed by plasma-assisted doping. *Appl. Phys. Lett.* 103:142110. doi: 10.1063/1.4824205
- Chen, S., Mahmoodi, M. R., Shi, Y., Mahata, C., Yuan, B., Liang, X., et al. (2020). Wafer-scale integration of two-dimensional materials in high-density memristive crossbar arrays for artificial neural networks. *Nat. Electron.* 3, 638–645. doi: 10.1038/s41928-020-00473-w
- Cheng, L., Li, Y., Yin, K. S., Hu, S. Y., Su, Y. T., Jin, M. M., et al. (2019). Functional demonstration of a memristive arithmetic logic unit (MemALU) for in-memory computing. *Adv. Funct. Mater.* 29:1905660. doi: 10.1002/adfm.201905660
- Chia, X., and Pumera, M. (2018). Characteristics and performance of two-dimensional materials for electrocatalysis. *Nat. Catal.* 1, 909–921. doi: 10.1038/s41929-018-0181-7
- Choi, S., Yang, J., and Wang, G. (2020). Emerging memristive artificial synapses and neurons for energy-efficient neuromorphic computing. *Adv. Mater.* 32:2004659. doi: 10.1002/adma.202004659
- Dai, H. N., Zheng, Z., and Zhang, Y. (2019). Blockchain for internet of things: a survey. *IEEE Internet Things J.* 6, 8076–8094. doi: 10.1109/JIOT.2019.2920987
- Esfandiari, M., Kamaei, S., Rajabali, M., and Mohajerzadeh, S. (2020). Formation of few- and monolayered WS₂ sheets using plasma-treated dimethyl-sulfoxide solvent-based exfoliation. *Phys. Status Solidi RRL* 14:1900396. doi: 10.1002/pssr.201900396
- Esfandiari, M., and Mohajerzadeh, S. (2019). Formation of large area WS₂ nanosheets using an oxygen-plasma assisted exfoliation suitable for optical devices. *Nanotechnology* 30:425204. doi: 10.1088/1361-6528/ab31b5
- Giannazzo, F., Fischella, G., Greco, G., Di Franco, S., Deretzis, I., La Magna, A., et al. (2017). Ambipolar MoS₂ transistors by nanoscale tailoring of schottky barrier using oxygen plasma functionalization. *ACS Appl. Mater. Interfaces* 9, 23164–23174. doi: 10.1021/acsami.7b04919
- Hu, M., Graves, C. E., Li, C., Li, Y., Ge, N., Montgomery, E., et al. (2018). Memristor-based analog computation and neural network classification with a dot product engine. *Adv. Mater.* 30:1705914. doi: 10.1002/adma.201705914
- Ielmini, D., and Wong, H. S. P. (2018). In-memory computing with resistive switching devices. *Nat. Electron.* 1, 333–343. doi: 10.1038/s41928-018-0092-2
- Jain, S., Ranjan, A., Roy, K., and Raghunathan, A. (2018). Computing in memory with spin-transfer torque magnetic RAM. *IEEE Trans. VLSI Syst.* 26, 470–483. doi: 10.1109/TVLSI.2017.2776954
- Kuc, A., Zibouche, N., and Heine, T. (2011). Influence of quantum confinement on the electronic structure of the transition metal sulfide TS₂. *Phys. Rev. B* 83:245213. doi: 10.1103/PhysRevB.83.245213
- Kumar, S., Wang, X., Strachan, J. P., Yang, Y., and Lu, W. D. (2022). Dynamical memristors for higher-complexity neuromorphic computing. *Nat. Rev. Mater.* 7, 575–591. doi: 10.1038/s41578-022-00434-z
- Kwon, K. C., Baek, J. H., Hong, K., Kim, S. Y., and Jang, H. W. (2022). Memristive devices based on two-dimensional transition metal chalcogenides for neuromorphic computing. *Nano Micro Lett.* 14:58. doi: 10.1007/s40820-021-00784-3
- Li, L., Han, W., Pi, L., Niu, P., Han, J., Wang, C., et al. (2019). Emerging in-plane anisotropic two-dimensional materials. *InfoMat* 1, 54–73. doi: 10.1002/inf2.12005
- Li, S., Xu, L. D., and Zhao, S. (2018). 5G internet of things: a survey. *J. Ind. Inf. Integr.* 10, 1–9. doi: 10.1016/j.jii.2018.01.005
- Lin, P., Li, C., Wang, Z., Li, Y., Jiang, H., Song, W., et al. (2020). Three-dimensional memristor circuits as complex neural networks. *Nat. Electron.* 3, 225–232. doi: 10.1038/s41928-020-0397-9
- Liu, C., Chen, H., Wang, S., Liu, Q., Jiang, Y. G., Zhang, D. W., et al. (2020). Two-dimensional materials for next-generation computing technologies. *Nat. Nanotechnol.* 15, 545–557. doi: 10.1038/s41565-020-0724-3
- Liu, L., Kumar, S. B., Ouyang, Y., and Guo, J. (2011). Performance limits of monolayer transition metal dichalcogenide transistors. *IEEE Trans. Electron. Devices* 58, 3042–3047. doi: 10.1109/ted.2011.2159221
- Liu, Y., Huang, Y., and Duan, X. (2019). Van der waals integration before and beyond two-dimensional materials. *Nature* 567, 323–333. doi: 10.1038/s41586-019-1013-x
- Luo, Z. D., Xia, X., Yang, M. M., Wilson, N. R., Gruverman, A., and Alexe, M. (2020). Artificial optoelectronic synapses based on ferroelectric field-effect enabled 2D transition metal dichalcogenide memristive transistors. *ACS Nano* 14, 746–754. doi: 10.1021/acsnano.9b07687
- Mao, J. Y., Zhou, L., Zhu, X., Zhou, Y., and Han, S. T. (2019). Photonic memristor for future computing: a perspective. *Adv. Opt. Mater.* 7:1900766. doi: 10.1002/adom.201900766
- Sharma, T., and Kumre, L. (2020). Energy-efficient ternary arithmetic logic unit design in CNTFET technology. *Circ. Syst. Signal Process.* 39, 3265–3288. doi: 10.1007/s00034-019-01318-4
- Sun, L., Wang, Z., Jiang, J., Kim, Y., Joo, B., Zheng, S., et al. (2021). In-sensor reservoir computing for language learning via two-dimensional memristors. *Sci. Adv.* 7:eabg1455. doi: 10.1126/sciadv.abg1455
- Verma, N., Jia, H., Valavi, H., Tang, Y., Ozatay, M., Chen, L., et al. (2019). In-memory computing: advances and prospects. *IEEE Solid State Circ. Magazine* 11, 43–55. doi: 10.1109/MSSC.2019.2922889
- Wang, M., Cai, S., Pan, C., Wang, C., Lian, X., Zhuo, Y., et al. (2018). Robust memristors based on layered two-dimensional materials. *Nat. Electron.* 1, 130–136. doi: 10.1038/s41928-018-0021-4
- Wang, Z., Zeng, T., Ren, Y., Lin, Y., Xu, H., Zhao, X., et al. (2020). Toward a generalized bienenstock-cooper-munro rule for spatiotemporal learning via triplet-STDP in memristive devices. *Nat. Commun.* 11:1510. doi: 10.1038/s41467-020-15158-3
- Yang, Y., Du, H., Xue, Q., Wei, X., Yang, Z., Xu, C., et al. (2019). Three-terminal memtransistors based on two-dimensional layered gallium selenide nanosheets for potential low-power electronics applications. *Nano Energy* 57, 566–573. doi: 10.1016/j.nanoen.2018.12.057
- Yin, L., Cheng, R., Wang, Z., Wang, F., Sendeku, M. G., Wen, Y., et al. (2020). Two-dimensional unipolar memristors with logic and memory functions. *Nano Lett.* 20, 4144–4152. doi: 10.1021/acs.nanolett.0c00002
- Yue, Y. C., Chen, J. C., Zhang, Y., Ding, S. S., Zhao, F. L., Wang, Y., et al. (2018). Two-dimensional high-quality monolayered triangular WS₂ flakes for field-effect transistors. *ACS Appl. Mater. Interfaces* 10, 22435–22444. doi: 10.1021/acsami.8b05885
- Zavabeti, A., Jannat, A., Zhong, L., Haidry, A. A., Yao, Z., and Ou, J. Z. (2020). Two-dimensional materials in large-areas: synthesis, properties and applications. *Nano Micro Lett.* 12:66. doi: 10.1007/s40820-020-0402-x
- Zhang, W., Huang, Z., Zhang, W., and Li, Y. (2014). Two-dimensional semiconductors with possible high room temperature mobility. *Nano Res.* 7, 1731–1737. doi: 10.1007/s12274-014-0532-x
- Zhong, Y., Tang, J., Li, X., Gao, B., Qian, H., and Wu, H. (2021). Dynamic memristor-based reservoir computing for high-efficiency temporal signal processing. *Nat. Commun.* 12:408. doi: 10.1038/s41467-020-20692-1
- Zhou, Z., Yang, F., Wang, S., Wang, L., Wang, X., Wang, C., et al. (2021). Emerging of two-dimensional materials in novel memristor. *Front. Phys.* 17:23204. doi: 10.1007/s11467-021-1114-5
- Zhu, L., Yu, F. R., Wang, Y., Ning, B., and Tang, T. (2019). Big data analytics in intelligent transportation systems: a survey. *IEEE Trans. Intell. Transp.* 20, 383–398. doi: 10.1109/TITS.2018.2815678